CLNS 04/1895
CLEO 04-14

Search for $e^+e^- \to \Lambda_b^0\overline{\Lambda}_b^0$ Near Threshold

D. Besson,[1] T. K. Pedlar,[2] D. Cronin-Hennessy,[3] K. Y. Gao,[3] D. T. Gong,[3] Y. Kubota,[3] B. W. Lang,[3] S. Z. Li,[3] R. Poling,[3] A. W. Scott,[3] A. Smith,[3] C. J. Stepaniak,[3] S. Dobbs,[4] Z. Metreveli,[4] K. K. Seth,[4] A. Tomaradze,[4] P. Zweber,[4] J. Ernst,[5] A. H. Mahmood,[5] K. Arms,[6] K. K. Gan,[6] H. Severini,[7] D. M. Asner,[8] S. A. Dytman,[8] W. Love,[8] S. Mehrabyan,[8] J. A. Mueller,[8] V. Savinov,[8] Z. Li,[9] A. Lopez,[9] H. Mendez,[9] J. Ramirez,[9] G. S. Huang,[10] D. H. Miller,[10] V. Pavlunin,[10] B. Sanghi,[10] E. I. Shibata,[10] I. P. J. Shipsey,[10] G. S. Adams,[11] M. Chasse,[11] M. Cravey,[11] J. P. Cummings,[11] I. Danko,[11] J. Napolitano,[11] C. S. Park,[12] W. Park,[12] J. B. Thayer,[12] E. H. Thorndike,[12] T. E. Coan,[13] Y. S. Gao,[13] F. Liu,[13] R. Stroynowski,[13] M. Artuso,[14] C. Boulahouache,[14] S. Blusk,[14] J. Butt,[14] E. Dambasuren,[14] O. Dorjkhaidav,[14] J. Li,[14] N. Menaa,[14] R. Mountain,[14] H. Muramatsu,[14] R. Nandakumar,[14] R. Redjimi,[14] R. Sia,[14] T. Skwarnicki,[14] S. Stone,[14] J. C. Wang,[14] K. Zhang,[14] S. E. Csorna,[15] G. Bonvicini,[16] D. Cinabro,[16] M. Dubrovin,[16] A. Bornheim,[17] S. P. Pappas,[17] A. J. Weinstein,[17] J. L. Rosner,[18] R. A. Briere,[19] G. P. Chen,[19] T. Ferguson,[19] G. Tatishvili,[19] H. Vogel,[19] M. E. Watkins,[19] N. E. Adam,[20] J. P. Alexander,[20] K. Berkelman,[20] D. G. Cassel,[20] V. Crede,[20] J. E. Duboscq,[20] K. M. Ecklund,[20] R. Ehrlich,[20] L. Fields,[20] R. S. Galik,[20] L. Gibbons,[20] B. Gittelman,[20] R. Gray,[20] S. W. Gray,[20] D. L. Hartill,[20] B. K. Heltsley,[20] D. Hertz,[20] L. Hsu,[20] C. D. Jones,[20] J. Kandaswamy,[20] D. L. Kreinick,[20] V. E. Kuznetsov,[20] H. Mahlke-Krüger,[20] T. O. Meyer,[20] P. U. E. Onyisi,[20] J. R. Patterson,[20] D. Peterson,[20] J. Pivarski,[20] D. Riley,[20] A. Ryd,[20] A. J. Sadoff,[20] H. Schwarthoff,[20] M. R. Shepherd,[20] S. Stroiney,[20] W. M. Sun,[20] J. G. Thayer,[20] D. Urner,[20] T. Wilksen,[20] M. Weinberger,[20] S. B. Athar,[21] P. Avery,[21] L. Breva-Newell,[21] R. Patel,[21] V. Potlia,[21] H. Stoeck,[21] J. Yelton,[21] P. Rubin,[22] C. Cawlfield,[23] B. I. Eisenstein,[23] G. D. Gollin,[23] I. Karliner,[23] D. Kim,[23] N. Lowrey,[23] P. Naik,[23] C. Sedlack,[23] M. Selen,[23] J. J. Thaler,[23] J. Williams,[23] J. Wiss,[23] and K. W. Edwards[24]

(CLEO Collaboration)

[1]*University of Kansas, Lawrence, Kansas 66045*
[2]*Luther College, Decorah, Iowa 52101*
[3]*University of Minnesota, Minneapolis, Minnesota 55455*
[4]*Northwestern University, Evanston, Illinois 60208*
[5]*State University of New York at Albany, Albany, New York 12222*
[6]*Ohio State University, Columbus, Ohio 43210*
[7]*University of Oklahoma, Norman, Oklahoma 73019*
[8]*University of Pittsburgh, Pittsburgh, Pennsylvania 15260*
[9]*University of Puerto Rico, Mayaguez, Puerto Rico 00681*
[10]*Purdue University, West Lafayette, Indiana 47907*
[11]*Rensselaer Polytechnic Institute, Troy, New York 12180*
[12]*University of Rochester, Rochester, New York 14627*
[13]*Southern Methodist University, Dallas, Texas 75275*
[14]*Syracuse University, Syracuse, New York 13244*
[15]*Vanderbilt University, Nashville, Tennessee 37235*

[16]*Wayne State University, Detroit, Michigan 48202*
[17]*California Institute of Technology, Pasadena, California 91125*
[18]*Enrico Fermi Institute, University of Chicago, Chicago, Illinois 60637*
[19]*Carnegie Mellon University, Pittsburgh, Pennsylvania 15213*
[20]*Cornell University, Ithaca, New York 14853*
[21]*University of Florida, Gainesville, Florida 32611*
[22]*George Mason University, Fairfax, Virginia 22030*
[23]*University of Illinois, Urbana-Champaign, Illinois 61801*
[24]*Carleton University, Ottawa, Ontario, Canada K1S 5B6*
and the Institute of Particle Physics, Canada
(Dated: Nov. 22, 2004)

Abstract

Using the CLEO III detector at CESR we study e^+e^- collisions in the center-of-mass energy close to, or above, $\Lambda_b^0\overline{\Lambda}_b^0$ production threshold. We search for evidence of $\Lambda_b^0\overline{\Lambda}_b^0$ resonance production and set upper limits based on inclusive hadron production as a barometer of $\Lambda_b^0\overline{\Lambda}_b^0$ production.

I. INTRODUCTION

The Λ_b^0, consisting of b, u and d quarks, is the lowest-lying b-flavored baryon, about which comparatively little is known. Recently the CDF collaboration reported an improved measurement of the Λ_b^0 mass [1] of 5620.4 $\pm$ 1.6 $\pm$ 1.2 MeV. The lifetime has long been measured to be somewhat lower than theoretical expectations [2]. There is, however, no measurement available on the direct production of exclusive $\Lambda_b^0\overline{\Lambda}_b^0$ in e^+e^- annihilation. Such events would be very useful for establishing absolute branching ratios and other properties. CLEO has accumulated data using e^+e^- collisions in the center-of-mass energy range from 11.227 to 11.383 GeV, close to or just above the $\Lambda_b^0\overline{\Lambda}_b^0$ production threshold. It is possible to observe a resonant signal, similar to the $\Upsilon(4S)$ for B^+ and B^0 mesons, or just an increase in relative production above threshold. We report here limits on such resonant or non-resonant production.

II. DATA AND MONTE CARLO SIMULATED SAMPLE

The CLEO III detector is described in detail elsewhere [3] [4]. The inner part of the detector is surrounded by a 1.5 T solenoidal magnetic field. From the region near the e^+e^- interaction vertex radially outward it consists of a silicon strip based vertex detector and a drift chamber used to measure the momenta of charged tracks based on their curvature. Beyond the drift chamber is a Ring Imaging Cherenkov Detector, RICH, used to identify charged hadrons, followed by an Electromagnetic Calorimeter, EC, consisting of nearly 8000 CsI crystals. Next to the EC there is the solenoidal coil followed by an iron return path with wire chambers interspersed in 3 layers to provide muon identification.

This study is based on the total 710 pb^{-1} data sample that was acquired at 3 MeV intervals between center-of-mass energies, E_{CM}, of 11.227 GeV to 11.383 GeV, to be close to or above threshold for $\Lambda_b^0\overline{\Lambda}_b^0$ production. The luminosity in each of these scan points varies from 14 to 20 pb^{-1}. In addition, there are data points taken at a E_{CM} of 11.150 and 11.203 GeV, respectively. The two data points with lowest and highest energies have integrated luminosities of 70 and 120 pb^{-1}, respectively. We also use data taken in the four-flavor continuum below the $\Upsilon(4S)$ to measure the $b\overline{b}$ cross section above the $\Upsilon(4S)$.

For the Monte Carlo, MC, study of the high energy data, we generated five times more hadronic $q\overline{q}$ events than at each beam energy contained in our data sample. Events were generated separately for "light" four-flavor continuum (c, s, u, d) and $b\overline{b}$ continuum events and then combined in the expected 10:1 ratio absent any resonance production. The decay channels and the branching fractions of the Λ_b are less well known than the B^0 and B^+ mesons. We list the Λ_b decay modes and branching fractions we used for the signal Monte Carlo in Table I. For the $\Lambda_b^0 \to \Lambda_c^+\ell^-\bar{\nu}$ branching fraction we re-scaled the $B^0 \to X\ell\bar{\nu}$ branching fraction by the ratio of lifetimes, $\tau(\Lambda_b)/\tau(B^0)$. The entries denoted by *$q\bar{q}$* indicate that the processes are generated using a fragmentation process for the quark-antiquark pair.

TABLE I: Λ_b decay modes and branching fractions used in the Monte Carlo simulation.

Decay modes	Branching fraction (%)
$\Lambda_b \to \Lambda_c^+ e^- \nu_e$	8.4
$\Lambda_b \to \Lambda_c^+ \mu^- \nu_\mu$	8.4
$\Lambda_b \to \Lambda_c^+ \pi^-$	4.2
$\Lambda_b \to \Lambda_c^+ \rho^-$	1.0
$\Lambda_b \to \Lambda_c^+ a1^-$	2.1
$\Lambda_b \to \Lambda_c^+ D_s^-$	2.1
$\Lambda_b \to \Lambda_c^+ D_s^{*-}$	4.2
$\Lambda_b \to \Lambda \eta_c$	0.1
$\Lambda_b \to \Lambda J/\psi$	0.5
$\Lambda_b \to \Lambda_c^+ \pi^- \pi^+ \pi^-$	2.1
$\Lambda_b \to \Lambda K^0 \pi^- \pi^- \pi^+ \pi^-$	2.1
$\Lambda_b \to p^+ D^0 \pi^-$	2.1
$\Lambda_b \to \Lambda_c^+ * d\overline{u}*$	44.9
$\Lambda_b \to \Sigma_c^+ * d\overline{u}*$	8.4
$\Lambda_b \to \Omega_{cc}^+ * d\overline{u}*$	7.3
$\Lambda_b \to p^+ * d\overline{u}*$	1.1
$\Lambda_b \to \Xi_c'^+ * d\overline{u}*$	1.0

III. EVENT SELECTION

The major backgrounds to Λ_b are non-$b\overline{b}$ type hadronic events, two-photon events ($e^+e^- \to e^+e^- X$) and $\tau^+\tau^-$ pairs. To suppress these backgrounds we require the following hadronic event selection criteria:

(1) At least five charged tracks; a track candidate is acceptable if it is a cosine with respect to the beam line of less than 0.9 and has at least half of the potential tracking chamber hits along its length. This requirement rejects 81% of the $\tau^+\tau^-$ pairs.

(2) The total visible energy, E_{vis}, is required to be greater than the beam energy, E_{beam}. E_{vis} receives contributions from both charged tracks and unmatched neutral energy clusters greater than 30 MeV. This requirement helps suppresses two-photon events. Fig. 1(a) shows the E_{vis}/E_{beam} distributions for data, five flavor Monte-Carlo continuum and simulated two-photon events [5]. Imposing the requirement $E_{vis} > E_{beam}$ reduces the two-photon background by 75% with a small (3%) loss of hadronic events.

(3) The ratio of the 2^{nd} and 0^{th} Fox-Wolfram moments, R_2, is less than 0.25 [6]. Fig. 1(b) shows MC simulated distributions of R_2 for both $b\overline{b}$ and non-$b\overline{b}$ continuum events. Both areas are normalized to unity. Requiring $R_2 < 0.25$ selects the more spherically shaped events in momentum space and greatly enhances the $b\overline{b}$ fraction, by rejecting 65% of four-flavor continuum events while losing only 8% of the $b\overline{b}$ events.

To subtract four-flavor continuum background we use data taken at a E_{CM} 30 MeV below the $\Upsilon(4S)$ mass. Since we make a specific cut on R_2 we need to take into account that the shape of the R_2 distribution can change when the E_{CM} changes. The R_2 distribution from

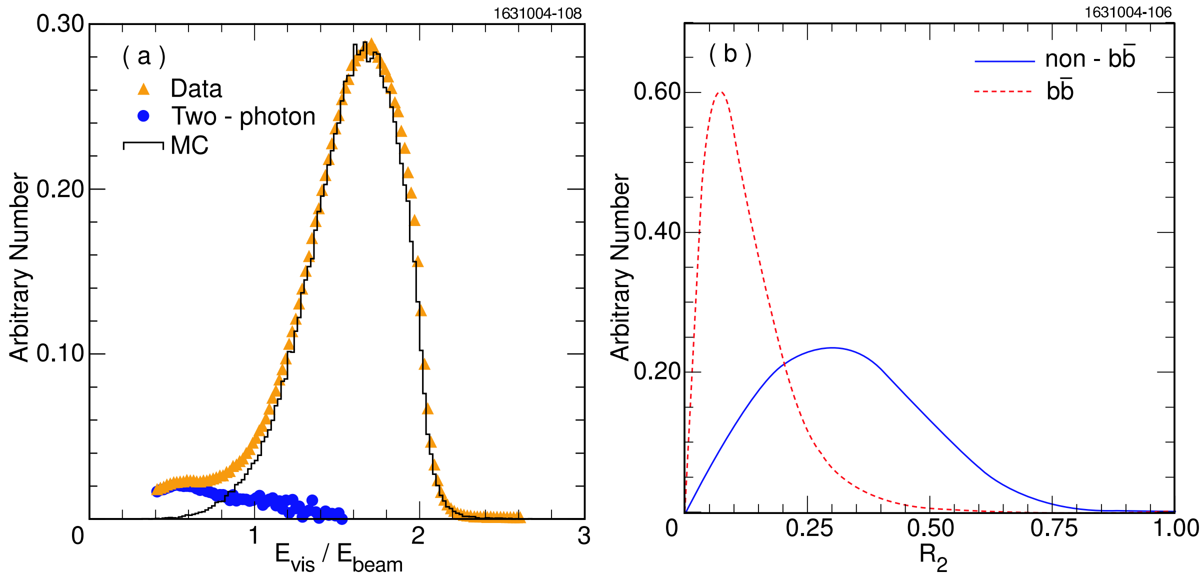

FIG. 1: (a) E_{vis}/E_{beam} above Λ_b threshold data (triangle), five flavor continuum MC (solid) and simulated two-photon events (circles). (b) R_2 distribution for $b\bar{b}$ (dashed) and non-$b\bar{b}$ (solid) type events.

below-$\Upsilon(4S)$ data is compared with the distribution using data taken in the Λ_b scan region in Fig. 2(a). The data are normalized by luminosity and $1/s$, where s is the square of the center-of-mass energy. The distributions differ in two respects. The first is the obvious enhancement at small R_2 values in the Λ_b scan region giving evidence for $b\bar{b}$ production. The second is the disagreement in shape at values of $R_2 > 0.5$, where $b\bar{b}$ production is absent.

We confirm this change in shape with energy by comparing $\Upsilon(4S)$ "on-resonance" data and below-$\Upsilon(1S)$ resonance data (E_{CM}=9.43 GeV) in Fig. 2(b). The subtracted spectra show an anomalous peak near $R_2 = 0.5$. The number of events in this peak can be as large as $\sim$30% of the total number of $b\bar{b}$ events in higher E_{CM} region. Thus, it is important to transform correctly the below-$\Upsilon(4S)$ resonance data in order to correctly subtract the background when we apply a tight R_2 requirement. Simple kinematic considerations suggest that $R_2'(E')/R_2(E) \sim E'/E$, where $E' > E$. The boundary considerations that at R_2 values of both 0 and 1 the initial and corrected distributions be equal, result in a simple parameterization of the corrected, or "boosted" R_2 distribution:

$$R_2'(E') = \frac{E'}{E} R_2(E) + \left(1 - \frac{E'}{E}\right) R_2^2(E) \ . \tag{1}$$

This expression describes the energy dependence of the R_2 shape excellently. In Fig. 3 we compare the boosted R_2 distribution for below-$\Upsilon(4S)$ data, normalized by luminosity and $1/s$, with the same distribution for the high energy data. The distributions match above R_2 of 0.5, as required.

We have several strategies for observing the production of $\Lambda_b^0\overline{\Lambda}_b^0$ events. One possibility is to look for enhancements in the (1) $b\bar{b}$ cross-section. Another is to look for an increase in (2) Λ or (3) anti-proton production. We don't use protons because there is a large background rate from hadron interactions in the beam pipe and from residual beam gas

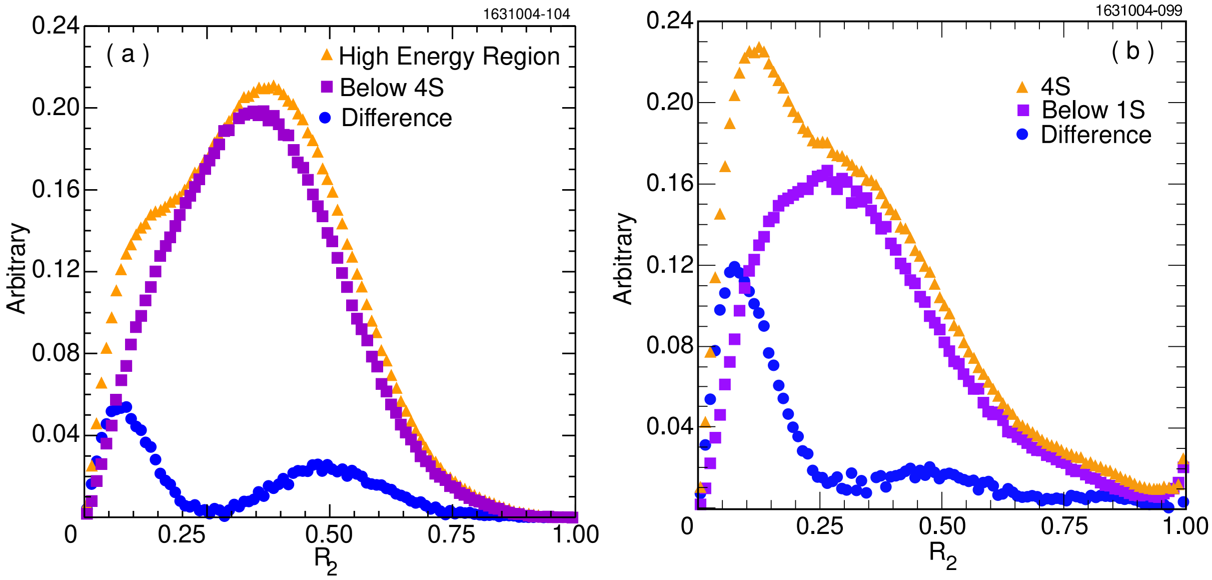

FIG. 2: The R_2 distribution above Λ_b threshold compared with below-$\Upsilon(4S)$ data (a) and $\Upsilon(4S)$ on resonance data compared with below-$\Upsilon(1S)$ data (b). Circles show the subtracted distributions.

collisions. Λ's are promising because we expect that $\Lambda_b^o \to \Lambda_c X$ has a large branching ratio, ~96% and $\Lambda_c^+ \to \Lambda X$ is approximately 50%. Detecting anti-protons is very promising because Λ_b^0 decays always produce either one proton or neutron. In the case of non-resonant $\Lambda_b^0\overline{\Lambda}_b^0$ production we can expect that the cross-section will increase from zero at threshold to some constant fraction of the total $b\bar{b}$ cross-section. In order to ascertain an optimal search strategy, we assume this fraction is 7.9%, as predicted by the JETSET 7.3 Monte

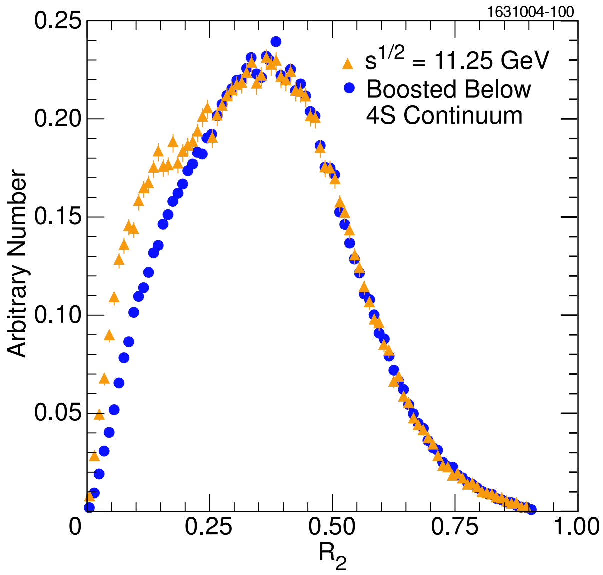

FIG. 3: R_2 Distribution at one energy point above Λ_b threshold compared with below-$\Upsilon(4S)$ after the boost (data).

Carlo model [7]. This is consistent with the PDG value for $b\bar{b} \to$ baryon of 10% [8]. Further support for this value comes from the ratio of $\Lambda_c\overline{\Lambda}_c$ to $c\bar{c}$ rates. As input to this estimate we use a measured value of $\mathcal{B}(\Lambda_c^+ \to pK^-\pi^+) \times \sigma(\Lambda_c^+) = (10.0 \pm 1.5 \pm 1.5)$ pb [9], from our below-$\Upsilon(4S)$ continuum data sample. We take the $c\bar{c}$ cross section as 4/10 of the total hadronic cross section, implying $\sigma(c\bar{c}) = 1.12 \pm 0.02$ nb [10], and we use the PDG mean value for $\mathcal{B}(\Lambda_c^+ \to pK^-\pi^+) = (5.0 \pm 1.3)\%$ [8], yielding the ratio or $\Lambda_c\overline{\Lambda_c}/c\bar{c} = (8.9 \pm 3.0)\%$.

The relative size of the $\Lambda_b^0\overline{\Lambda}_b^0$ component for our different search strategies is shown in Fig. 4(a). Here we normalized the MC simulated five-flavor visible hadronic cross section to unity, defined here as "continuum" $udsc$ and b, and then added the signal $\Lambda_b^0\overline{\Lambda}_b^0$ to the total $udscb$ cross section(i.e., the $\Lambda_b^0\overline{\Lambda}_b^0$ enhancement here represents an additional 7.9% above expected inclusive $b\bar{b}$ hadronic cross-section, rather than simply presenting an additional channel available to $b\bar{b}$ hadronization). Λ's have the highest relative yield closely followed by anti-protons. We optimize our search criteria by maximizing signal divided by square root of the background, $S/\sqrt{B}$, for our different search methods. The results are summarized in Fig. 4(b), where we show the statistical significance for signal we obtain for different analysis strategies for different $\Lambda_b^0\overline{\Lambda}_b^0$ cross-sections (statistical errors only).

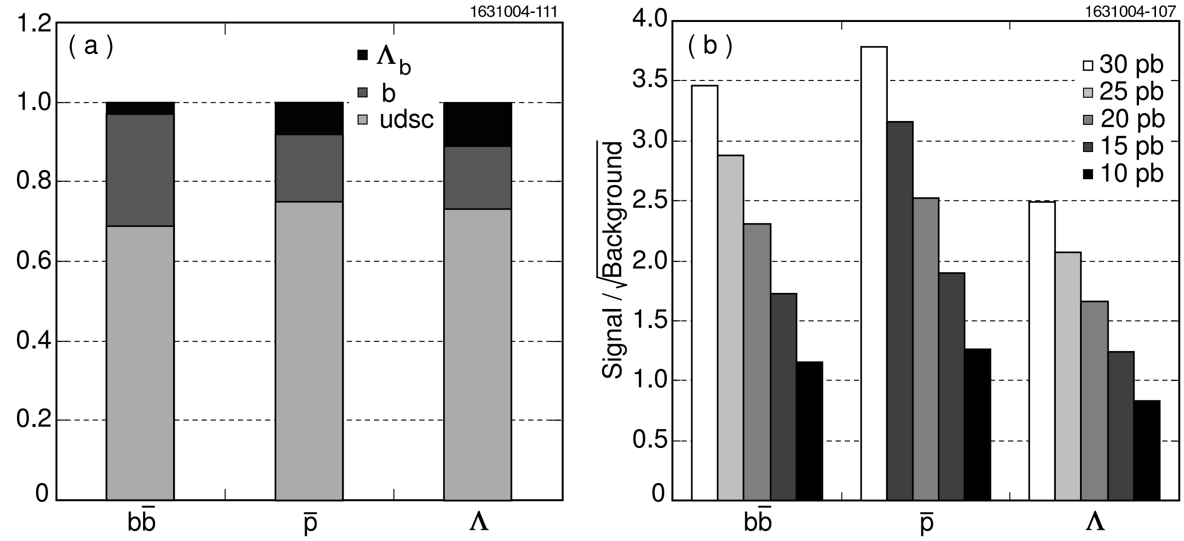

FIG. 4: (a) Relative yield of the $udsc$ (lower), b (middle) and Λ_b (upper) visible cross section for the inclusive selection of $b\bar{b}$, $\bar{p}$ and Λ assuming a 7.9% increase of the total $b\bar{b}$ cross section above $\Lambda_b^0\overline{\Lambda}_b^0$ threshold. (b) Signal/$\sqrt{\text{Background}}$ for different analysis strategies and cross-sections.

Our studies indicate that baryon production (namely anti-protons and Λ's) is the most sensitive measure of $\Lambda_b^0\overline{\Lambda}_b^0$. However, the systematic uncertainties in $\Lambda_b \to$ protons and $\Lambda_b \to \Lambda$ diminish their sensitivity relative to inclusive $b\bar{b}$ production. We also considered identifying Λ's and protons with an additional lepton in the event but these methods offer less significance. The efficiencies for detecting hadronic events, and more importantly, for detecting events with one or more protons are listed in Table II; their evaluation will be discussed in more detail in the next section.

We use both charged particle ionization loss in the drift chamber (dE/dx) and RICH information to identify anti-protons. The RICH is used for momenta larger than 1 GeV.

Information on the angle of detected Cherenkov photons is translated into a likelihood of a given photon being due to a particular particle. Contributions from all photons associated with a particular track are then summed to form an overall likelihood denoted as $\mathcal{L}_i$ for each particle hypothesis. To differentiate between kaon and proton candidates, we use the difference: $-\log(\mathcal{L}_K) + \log(\mathcal{L}_{proton})$. This cut is set at -4. To utilize the dE/dx information we calculate σ_K as the difference between the expected ionization loss for a kaon and the measured loss divided by the measurement error. Similarly, σ_{proton} is defined in the same manner using the expected ionization for a proton.

We use both the RICH and dE/dx to select anti-proton candidates in the following manner: (a) If neither the RICH nor dE/dx information is available, then the track is rejected. (b) If dE/dx is available and RICH is not then we insist that proton candidates have $PID_{dE} \equiv \sigma_K^2 - \sigma_{proton}^2 < 0$ (c) If RICH information is available and dE/dx is not available, then we require that $PID_{RICH} \equiv -\log(\mathcal{L}_K) + \log(\mathcal{L}_{proton}) < -4$. (d) If both dE/dx and RICH information are available, we require that $(PID_{dE} + PID_{RICH}) < -4$.

Λ candidates are formed from a pair of oppositely charged tracks one of which is consistent with a proton or anti-proton hypothesis, with a looser criteria than that stated above, which are constrained to come from a single vertex. We also require that the invariant mass be within 5 times the width of the Λ mass peak, which has an r.m.s. width of 1.4 MeV.

A. Efficiency Determinations

To derive event selection efficiencies we simulated hadronic events using the JETSET 7.3 $q\overline{q}$ event generator [11], then followed through the full GEANT 3.21-based [12] CLEO-III detector simulation. For five-flavor hadronic and $\Lambda_b^0\overline{\Lambda}_b^0$ events in the Λ_b scan region, we generated Monte Carlo samples using the same generator with the properties described in section II. The efficiencies obtained from these simulations are presented in Table II, where we list the both the hadronic event selection efficiency and the efficiency for detecting a hadronic event with an anti-proton. These efficiencies include the branching ratios for the various processes into anti-protons in the second column. We take $\mathcal{B}(\Lambda_b^o \to \overline{p}X) = 0.50$. The row for $b\overline{b}$ includes only B meson production with additional pions allowed. As one would expect, the efficiencies for $b\overline{b}$ and $\Lambda_b^0\overline{\Lambda}_b^0$ are very similar. The slightly lower efficiency for $\Lambda_b^0\overline{\Lambda}_b^0$ arises from higher average jettiness for $\Lambda_b^0\overline{\Lambda}_b^0$ events.

The errors listed in Table II are statistical and systematic, respectively. The systematic error for the hadronic event selection requirement is estimated from the variation in the number of hadronic events (corrected by efficiency and background) when changing selection requirements. The systematic error for the proton identification has been evaluated from proton efficiency measurements using reconstructed Λ events from data and then comparing with the equivalent MC estimation.

Our simulations also give us the selection efficiency for detecting an event containing either a Λ or an $\overline{\Lambda}$ from $\Lambda_b\overline{\Lambda}_b$ decay of $16.6 \pm 0.1^{+1.0}_{-0.0}\%$, including the $\mathcal{B}(\Lambda \to p\pi^-)$. Note that the PDG world average for $\mathcal{B}(\Lambda_c \to p \text{ anything})$ of (50 ± 16). Similarly $\mathcal{B}(\Lambda_c \to \Lambda \text{ anything})$ is $(35 \pm 11)\%$ [8]. The errors on these rates will be included separately as systematic effects.

TABLE II: Selection efficiencies for hadronic events and those with anti-protons.

Data samples	Selection efficiency for hadronic events (%)	Selection efficiency for hadronic events with an $\overline{p}$ (%)
Below-$\Upsilon(4S)$ continuum	25.5 $\pm$ 0.2 $\pm$ 0.8	2.1 $\pm$ 0.1 $\pm$ 0.1
$\Lambda_b^0\overline{\Lambda}_b^0$	85.5 $\pm$ 0.9 $\pm$ 2.6	26.8 $\pm$ 0.1 $\pm$ 5.4
4 flavor ($udsc$) continuum at $E_{beam} \sim m(\Lambda_b)$	21.9 $\pm$ 0.4 $\pm$ 0.7	1.8 $\pm$ 0.2 $\pm$ 0.1
$b\overline{b}$	89.9 $\pm$ 1.2 $\pm$ 2.7	4.0 $\pm$ 0.2 $\pm$ 0.3
5 flavor ($udscb$) continuum	28.1 $\pm$ 2.5 $\pm$ 0.8	2.0 $\pm$ 0.3 $\pm$ 0.2
$\tau\overline{\tau}$	0.024 $\pm$ 0.005 $\pm$ 0.001	$< 10^{-5}$

B. Systematic Errors

The systematic errors in determining $\Lambda_b^0\overline{\Lambda}_b^0$ production are given in Table III. The largest error is due to the unknown branching fraction of $\mathcal{B}(\Lambda_c \to pX)$ to which we assign a 32% error. We also include errors on the hadron selection efficiency and the background in the hadronic event sample, evaluated by varying our selection criteria as well as taking into account the variation along E_{CM} change, the anti-proton identification efficiency evaluated by examining a larger sample of $\Lambda \to p\pi^-$ data, and the luminosity measurement uncertainty estimated as 1% [13].

The total systematic error found by adding these elements in quadrature is 2.7%, 32% and 31% on the determination of $\Lambda_b^0\overline{\Lambda}_b^0$ production using $b\overline{b}$, anti-protons and Λ's, respectively.

TABLE III: List of systematic errors in determining $\Lambda_b^0\overline{\Lambda}_b^0$ production

Source	Error (%)
Hadron efficiency	$\pm$3
$\Lambda_b^o \to \Lambda_c^+ X$ branching ratio	$\pm$4
Proton identification efficiency	$\pm$4
$\Lambda_c^+ \to pX$ branching fraction	$\pm$32
$\Lambda_c^+ \to \Lambda X$ branching fraction	$\pm$31
Total background of hadronic events	$\pm$2
Luminosity	$\pm$1

IV. THE ESTIMATED $b\overline{b}$ CROSS SECTION

The hadronic cross section is generally expressed in terms of its ratio R to the point cross section $e^+e^- \to \mu^+\mu^-$. To search for resonant or non-resonant production of $\Lambda_b^0\overline{\Lambda}_b^0$ in e^+e^-

collisions we measure the $b\bar{b}$ cross section over the energy range of the scan. Theoretically, $R_{b\bar{b}}$ can be expressed as follows:

$$R_{b\bar{b}} = R^0_{b\bar{b}} \left[1 + \alpha_s/\pi + C_2(\alpha_s/\pi)^2 + C_3(\alpha_s/\pi)^3 \right], \tag{2}$$

where $R^0_{b\bar{b}} = N_c q_b$. N_c is the number of quark colors, q_b is the b quark charge and α_s is the strong coupling constant. The constants are $C_2 = 1.409$ and $C_3 = -11.767$ [14]. In our energy regime, we expect a value for $R_{b\bar{b}}$ of 0.35.

To find the $b\bar{b}$ cross section we subtract the R_2 four-flavor continuum data distribution from the higher energy data, correct for the efficiency of the R_2 cut and the hadronic selection criteria and divide by the relevant luminosity. We use a value of the cross-section for $e^+e^- \to \mu^+\mu^-$ equal to 86.8 nb/s, where s is the square of the center-of-mass energy in units of GeV. However, we do not make a precise measurement of $b\bar{b}$ cross section due to uncertainties in the correct scaling factors of two-photon events and initial state radiation contributions in different energy regions. Here we wish to measure any possible enhancement above the $\Lambda_b^0\overline{\Lambda}_b^0$ threshold. Our results are presented in Fig. 5 (a).

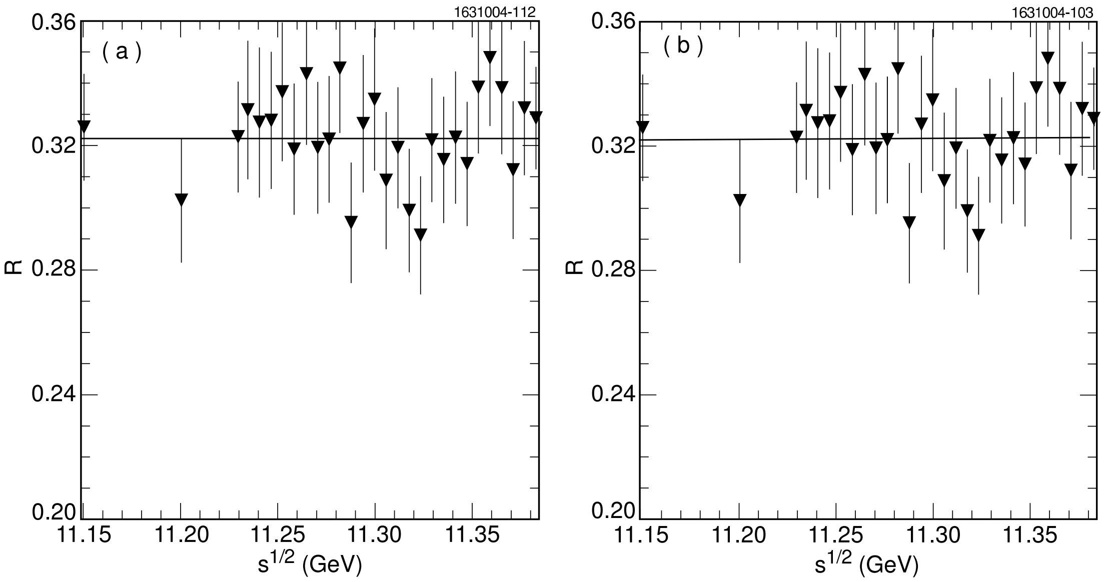

FIG. 5: The estimated $b\bar{b}$ cross section in units of R. The error bars on the data points represent both the statistical and the systematic errors summed in quadrature. (a) The solid line shows a fit to a horizontal line. (b) The solid line shows a fit to Equation 3. The fits are described in the text.

V. UPPER LIMITS ON Λ_b PRODUCTION

In this energy regime we expect that the R value will be constant in the absence of any resonant or threshold increase due to $\Lambda_b^0\overline{\Lambda}_b^0$ production. There are no statistically significant excesses above a constant value of R, suggesting no resonant production of $b\bar{b}$ types of events. There is an important caveat concerning the limit using the $b\bar{b}$ cross-section. It may very well be that opening up the $\Lambda_b^0\overline{\Lambda}_b^0$ channel comes at the expense of a lower in rate of other channels so that the total $b\bar{b}$ rate remains constant. Should this occur our limit, in this ($b\bar{b}$) case, would be meaningless. In fact, a fit to flat line for $b\bar{b}$ yields a χ^2 of 14.2 for 29 degrees of freedom. This fit is shown on Fig. 5 (a).

We can look for an increase in $\Lambda_b^0\overline{\Lambda}_b^0$ production that mimics the threshold turn on as a function of center-of-mass energy of $e^+e^- \to \tau^+\tau^-$. The lower line in Fig. 5 (b) represents a two-component fit. The first component is a straight line without any slope allowed up to a E_{CM} of 11.24 GeV, twice the Λ_b mass. The second component uses a shape similar to one proposed by the BES collaboration [15], but simplified by explicitly calculating the Coulomb interaction and final state radiation; the final form of this function is:

$$\sigma(s) = A \times \theta(\sqrt{s} - 2m(\Lambda_b^0)(\sqrt{s} - 2m(\Lambda_b^0))^{0.62} + R_0 \quad , \tag{3}$$

where A is a fit parameter, $\theta(y)$ is step function, 0 for y<0 and 1 for y> 0, $m(\Lambda_b^0)$ is the mass and R_0 is the observed cross section below threshold. (We are assuming this form applies only near threshold.)

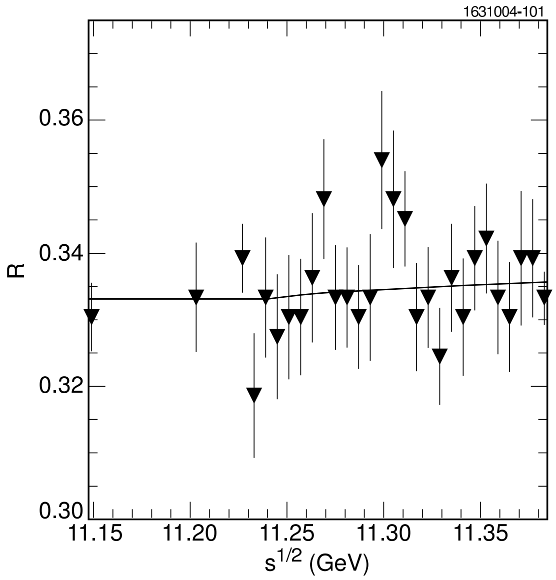

FIG. 6: The cross section for events with at least one anti-proton normalized by $\sigma(e^+e^- \to \mu^+\mu^-)$. (The data have not been corrected for hadronic event efficiencies.) The solid lines show fits to Equation 3. The errors are statistical only.

The cross sections for events with anti-protons is shown in Fig. 6. The data have been corrected for the momentum dependent efficiency of identifying anti-protons, but not for hadronic event selection. The data are fit to the BES function given in Eq. (3). The fitted parameters used to set upper limits are listed in Table IV.

The cross sections for events with Λ's is shown in Fig. 6. The data have been corrected for both Λ reconstruction efficiency and the branching ratio for $\Lambda_b^0\overline{\Lambda}_b^0$ into Λ plus $\overline{\Lambda}$. The fit to data uses the BES function given in Eq. (3). The fitted parameters used to set upper limits are listed in Table IV.

There is no significant resonance peak in the scan range, nor any evidence for a growth above threshold. Using these fits we calculate 95% confidence level upper limits for

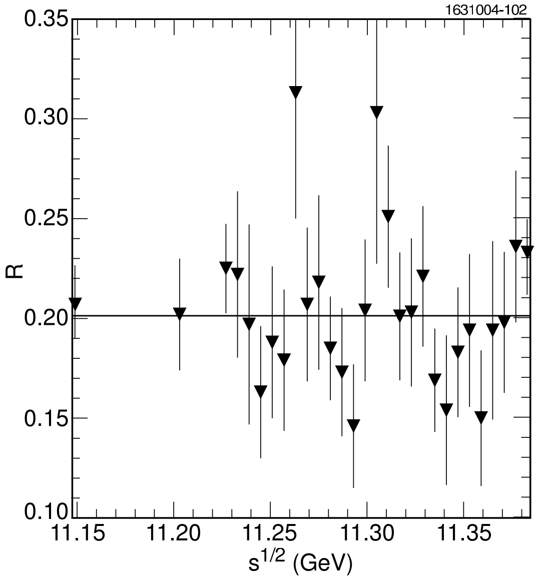

FIG. 7: (a) The cross section for events with at least one $\overline{\Lambda}$ normalized by $\sigma(e^+e^- \to \mu^+\mu^-)$. (The data have not been corrected for hadronic event efficiencies.)The solid lines show fits to Equation 3. The errors are statistical only.

$\Lambda_b^0\overline{\Lambda}_b^0$ production above threshold, as shown in Fig. 8. Here we take the upper limit as

$$\sigma(s)_i^{upper} = (A_i + 1.64 \times \delta A_i) * \left(\sqrt{s} - 2m(\Lambda_b^0)\right)^{0.62} / \epsilon_i \quad , \tag{4}$$

where A_i is the fit value from Table IV, δA_i is its error, ϵ_i is the relative Λ_b efficiency for each of the three different methods of 0.95, 0.29, and 0.86, for $b\bar{b}$, $\overline{p}$ and Λ searches, respectively. The 0.95 results from the relative efficiency of continuum $b\bar{b}$ production to $\Lambda_b\overline{\Lambda}_b$, the 0.27 is the product of the $\Lambda_b\overline{\Lambda}_b$ decay rate into anti-protons and the efficiency of the hadronic event selection, and the 0.86 is hadronic event selection for $\Lambda_b\overline{\Lambda}_b$. The systematic errors are included only in the limits using $b\bar{b}$ production. In the other two cases the systematic errors on the inclusive $\overline{p}$ and Λ branching ratios worsen the upper limits by 32% and 31%, respectively.

We determine upper limits for production of a resonance that would decay into $\Lambda_b^0\overline{\Lambda}_b^0$, similar in spirit to $\Upsilon(4S) \to B\overline{B}$. Here we take two possible intervals for either a narrow 6 MeV wide resonance or a wider, arbitrarily chosen, 18 MeV resonance. For the first case we

TABLE IV: Numerical values of parameters found by fitting Eq. 3 to our data.

Selection criteria	A_i	R_{0i}
$b\bar{b}$	$(0.21 \pm 3.82) \times 10^{-2}$	0.322 ± 0.007
Anti-proton	$(0.84 \pm 1.20) \times 10^{-2}$	0.333 ± 0.002
Λ	$(0.15 \pm 5.49) \times 10^{-2}$	0.201 ± 0.010
Twice the Λ_b mass is fixed to 11.24 GeV.		

fit a horizontal line to our data up to the $\Lambda_b^0\overline{\Lambda}_b^0$ threshold of 11.24 GeV and then estimate the upper limit for a cross-section excess in each 6 MeV interval of center of mass energy. These 95% confidence level upper limits are shown in Fig. 9(a).

For the second case, we fit all our data to a horizontal straight line while excluding an 18 MeV wide interval of center-of-mass energy. We then calculate the 95% confidence level upper limit by calculating the difference of the data relative to the fit line. These limits are shown in Fig. 9(b).

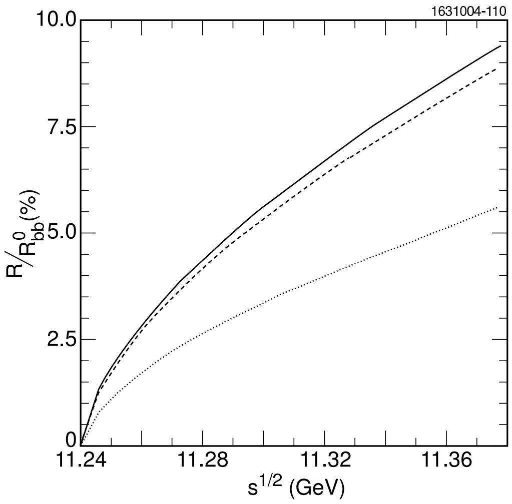

FIG. 8: The fractional upper limits at 95% c. l. for $\Lambda_b^0\overline{\Lambda}_b^0$ production obtained using Λ (solid line), anti-proton (dashed line) and the $b\bar{b}$ (dotted line) yields set by using the BES function. For the $b\bar{b}$ case only, systematic errors have been included.

No resonant enhancement reminiscent of the $\Upsilon(4S)$ resonance is observed. Using the threshold function we can set an upper limit at our highest energy point of 11.383 GeV on the ratio of Λ_b^0 to $b\bar{b}$ production. These limits are given in Table V. For $b\bar{b}$ production we use two values - the first is $R^0_{b\bar{b}}$ as defined in Eq. 2; the second is determined by fitting $R_{b\bar{b}}$ values assuming no enhancement along scan range. These values are $R^0_{b\bar{b}} = 1/3$ and $R_{b\bar{b}} = 0.322 \pm 0.004$.

The limits based on this function become lower toward lower energy as we approach the production threshold. The anti-proton and Λ samples are somewhat correlated in that anti-protons from $\overline{\Lambda}$ decay are often included in both samples, so we choose not to combine these limits.

VI. CONCLUSIONS

We do not observe any resonant or threshold enhancement of $\Lambda_b^0\overline{\Lambda}_b^0$ production in the center of mass energy region just above threshold, resulting in 95% confidence level upper limits on the order of 0.05-0.10 units of R. The 95% confidence level upper limits from anti-proton and Λ production are 12.8% and 12.9% of $R^0_{b\bar{b}}$, respectively, at our highest energy

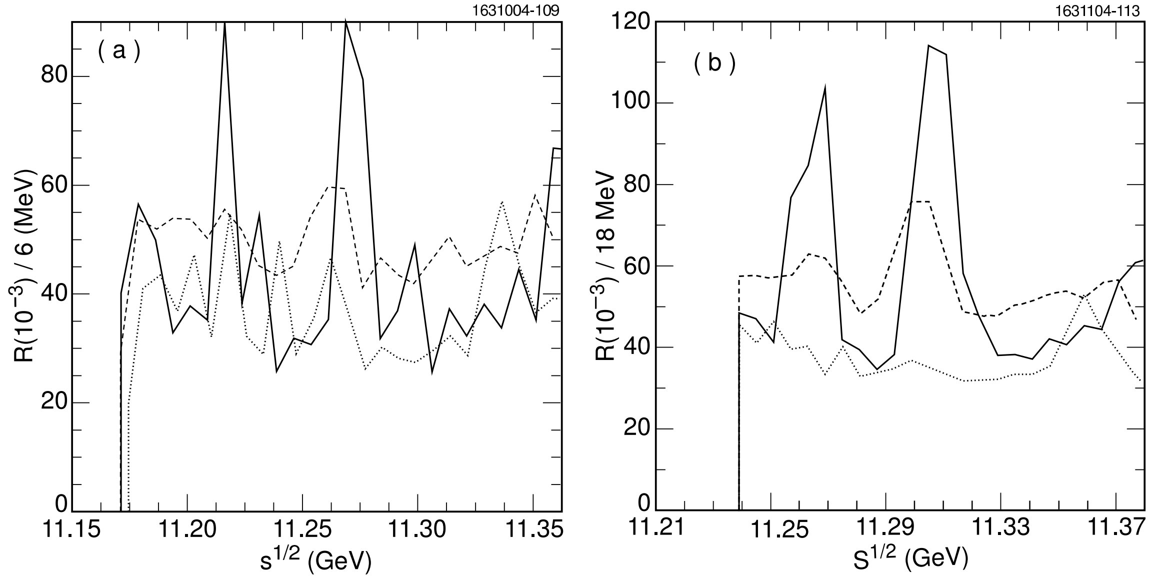

FIG. 9: Upper limits at 95% c. l. for $\Lambda_b^0\overline{\Lambda}_b^0$ production obtained using Λ (solid line), anti-proton (dashed line) and the $b\bar{b}$ (dotted line) yields. (a) The upper limits have been set in 6 MeV center of mass energy intervals in the scan region. (b) Upper limits in 18 MeV wide intervals. For the $b\bar{b}$ case only, systematic errors have been included.

point if they are modelled as a growth above threshold. In order to effectively study Λ_b decays at e^+e^- machines, it may be necessary to go to higher center of mass energies.

---

[1] K. Pitts, Int. J. Mod. Phys. **A19**, 991 (2004) [hep-ex/0312031].

[2] A Lenz, "Theoretical status of the lifetime predictions: $(\Delta\Gamma/\Gamma)_{B_s}, \tau_{B^+}/\tau_{B_d}$ and $\tau_{\Lambda_b}/\tau_{B_d}$," [hep-ph/0107033] (2001); N. Uraltsev, "Topics in the Heavy Quark Expansion," [hep-ph/0010328] (2001).

[3] CLEO Collaboration, S. Kopp *et al.*, Nucl. Instrum. Meth. A **384**, 61 (1996); A. Wolf *et al.*, Nucl. Instrum. Meth. A **408**, 58 (1998); G. Viehhauser *et al.*, Nucl. Instrum. Meth. A **462**, 146 (2001).

TABLE V: Upper limits at 95% c.l. on the ratio of $\Lambda_b^0\overline{\Lambda}_b^0$ to $b\bar{b}$ production at 11.383 GeV.

method	95% c.l. (statistical only)		95% c.l. (statistical & systematic)	
	$R_{\Lambda_b^0\overline{\Lambda}_b^0}/R^0_{b\bar{b}}$	$R_{\Lambda_b^0\overline{\Lambda}_b^0}/R_{b\bar{b}}$	$R_{\Lambda_b^0\overline{\Lambda}_b^0}/R^0_{b\bar{b}}$	$R_{\Lambda_b^0\overline{\Lambda}_b^0}/R_{b\bar{b}}$
$b\bar{b}$	-	-	6.0%	6.2%
Anti-proton	9.2%	9.5%	12.2%	12.5%
Λ	9.9%	10.2%	12.9%	13.3%

[4] CLEO Collaboration, R. Mountain *et al.*, Nucl. Instrum. Meth. A **433**, 77 (1999); M. Artuso *et al.*, Nucl. Instrum. Meth. A **502**, 91 (2003).

[5] The two-photon event simulation used in this study generates beam radiation according to the known probability function and uses the known energy dependence of $\gamma^*\gamma^* \to hadrons$. See O. Dorjkhaidav, thesis Syracuse University (2004), unpublished.

[6] G. C. Fox and S. Wolfram, Phys. Rev. Lett. **41** 1581 (1978).

[7] C. Weiser, "A measurement of the branching fractions of the b-quark into charged and neutral b-hadrons," DELPHI 2003-030 CONF 650 submitted to Lepton-Photon Conference (2003). The parameters of JETSET 7.3 are described in P. Abreu *et al.* (DELPHI), Z. Phys. **C73**, 11 (1996).

[8] S. Eidelman *et al.*, Phys. Letters **B592**, 1 (2004).

[9] CLEO Collaboration, P. Avery *et al.*, Phys. Rev. **D43**, 3599 (1991).

[10] R. Ammar *et al.* (CLEO), Phys. Rev. **D57**, 1350 (1998).

[11] S. J. Sjostrand, LUND 7.3, CERN Report No. CERN-TH-6488-92 (1992).

[12] R. Brun *et al.*, GEANT, version 3.14, CERN Report No. CERN CC/EE/84-1 (1987).

[13] CLEO Collaboration, B. Heltsley *et al.*, Nucl. Instrum. Meth. A **345**, 429 (1994).

[14] K. G. Chetyrkin *et al.*, Physics Reports **277**, 189 (1996).

[15] BES Collaboration, J. Z. Bai *et al.*, Phys. Rev. **D53**, 20 (1996).